PHYSICAL REVIEW B **84**, 041302(R) (2011)

# Electrically tuned *g* tensor in an InAs self-assembled quantum dot

R. S. Deacon,[1,2,*] Y. Kanai,[1] S. Takahashi,[1] A. Oiwa,[1,2] K. Yoshida,[1] K. Shibata,[3] K. Hirakawa,[2,3,4] Y. Tokura,[5] and S. Tarucha[1,4]

[1] *Department of Applied Physics, University of Tokyo, 7-3-1 Hongo, Bunkyo-ku, 113-8656, Japan*
[2] *JST CREST, 4-1-8 Hon-cho, Kawaguchi-shi, Saitama 332-0012, Japan*
[3] *Institute of Industrial Science, University of Tokyo, 4-6-1 Komaba, Meguro-ku, Tokyo 153-8505, Japan*
[4] *INQIE, University of Tokyo, 4-6-1 Komaba, Meguro-ku, Tokyo 153-8505, Japan*
[5] *NTT Basic Research Laboratories, NTT Corporation, Atsugi-shi, Kanagawa, 243-0198, Japan*

(Received 1 June 2011; published 6 July 2011)

We investigate the all-electrical tuning of the Landé $g$ tensor in a single uncapped InAs quantum dot contacted with a nanogap electrode technique and electrically gated with both back- and side-gate electrodes. Magnetotransport measurements allow extraction of the $g$ tensor components from measurements of the Zeeman energy for magnetic fields applied in the plane of the sample. The side-gate electrode allows tuning of the anisotropy of the in-plane $g$ tensor components and is suitable for the manipulation of the quantum-dot spin states using $g$ factor modulation resonance schemes.

DOI: 10.1103/PhysRevB.84.041302 PACS number(s): 73.63.Kv, 73.23.Hk

The spin of single carriers in semiconductor quantum dots (QDs) is one promising qubit for quantum information processing.[1] One basic operation in QD spin qubits requires the controlled rotation of a single spin,[1,2] which may be achieved with conventional electron spin resonance (ESR) utilizing a time-dependent magnetic field.[3] Selective addressing of a single qubit in an array requires either unique resonance frequencies for each qubit or a technique to generate a highly local time-dependent magnetic field. Many schemes for effective local magnetic field generation have been proposed, including control of the zero-field spin splitting[4,5] or using local gates to move a spin in a hyperfine field[6] or a slanting Zeeman field.[7,8] One candidate not yet realized in a single QD device is $g$-tensor modulation resonance (g-TMR), which requires local gate modulation of the $g$ tensor.[9,10] In two-dimensional devices, electrically tunable $g$ factors have been achieved using AlGaAs quantum wells grown with a graded composition.[11] This tunability has been exploited for $g$-TMR using a local time-dependent electric field to generate an effective time-dependent magnetic field for the manipulation of an ensemble of spins.[9] In single QD devices, strong confinement limits the tunability of the wave function. In self-assembled QDs grown through the Stranski-Krastanov (S-K) mode, only small variations in $g$ factor ($\sim 8\,\%$) with electrical gating have been reported.[12] In this Rapid Communication, we report strongly tunable Landé $g$ tensor in a single self-assembled InAs QD, achieved by gating the device with both a back-gate and anisotropic side-gate electrode.

Recently, high-resolution $e$-beam lithography techniques have allowed the contacting of single uncapped self-assembled QDs, grown by the S-K mode, with source and drain electrodes.[13–17] Furthermore, it has been shown that the confinement potential of self-assembled QD devices with relatively large lateral size may be efficiently tuned with an anisotropic side-gate electrode allowing tuning of the QD properties such as tunnel coupling Ref. 18 and spin-orbit energy Ref. 19. Measurements are performed on a single uncapped InAs QD contacted with titanium/aluminium (5/100 nm Ti/Al) nanogap electrodes. One back-gate electrode buried 300 nm below the sample surface and a side-gate electrode are used to charge and tune the states of the QD. A scanning electron microscope (SEM) image of the device is shown in Fig. 1(a). The device is the same as that studied in a previous paper,[18,19] however, the specific charge states studied in this paper are different because thermal cycling results in a change of device properties. For further details of the device fabrication, see Ref. 18. Measurements in this paper are performed at a temperature of 1.5 K using a single-axis rotating sample holder (accuracy $\pm 1^\circ$) allowing an applied external magnetic field to be orientated in any direction in the plane of the sample surface, as illustrated in Fig. 1(a).

Figure 1(b) shows a false color plot of the differential conductance ($G = dI/dV_{sd}$) as a function of source-drain bias ($V_{sd}$) and back-gate bias ($V_{bg}$) with constant side-gate bias ($V_{sg} = -2.0$ V). Throughout this paper, we focus on the properties of the charge state indicated by the charging diamond marked with white lines. Here, the QD is occupied by an odd electron number ($N$), as indicated by the presence of weak Kondo zero-bias anomalies [20] in regions $N$ and $N+2$, and the magnetic evolution of the Coulomb peaks [Fig. 1(c)]. The total electron number occupying the QD is unknown but likely to be a few tens of electrons. The charging energy is evaluated as $U \sim 4$ meV and the energy level spacing is $\sim$ 1–3 meV. From the stability diagram, we evaluate the back-gate lever arm $\alpha_{bg} = U/\Delta V_{bg}$, which relates the back-gate bias to the energy level of the QD. For $V_{sg} = -2.0$ V, we evaluate $\alpha = 0.11 \pm 0.01$ eV/V. Using the constant interaction model,[21] we extract the capacitances of the back-gate ($C_{bg}$) and source-drain electrodes ($C_{\mathrm{source}}$-$C_{\mathrm{drain}}$). The ground-state lines forming the edge of the Coulomb diamond [white lines in Fig. 1(a)] have gradients given by $C_{bg}/(C_\Sigma - C_{\mathrm{source}})$ and $-C_{bg}/C_{\mathrm{source}}$ where $C_\Sigma = (C_{\mathrm{source}} + C_{\mathrm{drain}} + C_{bg}) = e^2/U$. For $V_{sg} = -2.0$ V, we find that $C_{\mathrm{source}} = 23 \pm 3$ aF, $C_{\mathrm{drain}} = 13 \pm 3$ aF, $C_{bg} = 4.5 \pm 0.7$ aF, and $C_{sg} = 0.09 \pm 0.01$ aF.

Before detailed discussion of the variation in the $g$ tensor, we will consider the effects of $V_{sg}$ on the stability diagram in the region of interest. Figure 2(a) shows the Coulomb charging peaks as a function of $V_{bg}$ at $V_{sd} = 0$ V for a range of $V_{sg}$. As $V_{sg}$ is increased, a lower $V_{bg}$ is required to charge the QD. From stability diagrams at different $V_{sg}$, we extract $U$ and $\alpha_{bg}$

 

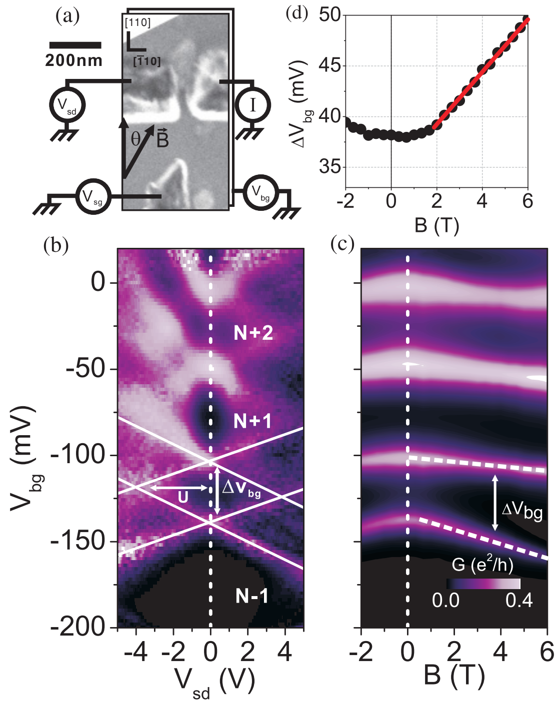


FIG. 1. (Color online) (a) SEM image of the device studied and schematic of the measurement setup. The QD is elongated along the [110] crystallographic axis. (b) Charging stability plot of the differential conductance ($G = dI/dV_{sd}$) as a function of $V_{bg}$ and $V_{sd}$ with $V_{sg} = -2.0$ V and $B = 0$ T. (c) Plot of the magnetic evolution of the Coulomb peaks ($\theta = 45°$). (b) and (c) are plotted with the same color scale shown in inset in (c). (d) Plot of $\Delta V_{bg}(B)$ extracted from (c). The solid line indicates a linear best fit used to evaluate $|g|$.

using the methods previously discussed and plot the results in Figs. 2(b) and 2(c). Increasing $V_{sg}$ leads to a decrease in $\alpha_{bg}$ and a decrease in $U$, as shown in Figs. 2(b) and 2(c). These observations are consistent with an observed increase of the source-drain and back-gate capacitances.[20] Overall, these features indicate a shift of the confined states toward the source-drain electrodes and back gate for a positive $V_{sg}$ and away for a negative $V_{sg}$, which is consistent with the orientation of the side gate and QD with respect to the source-drain

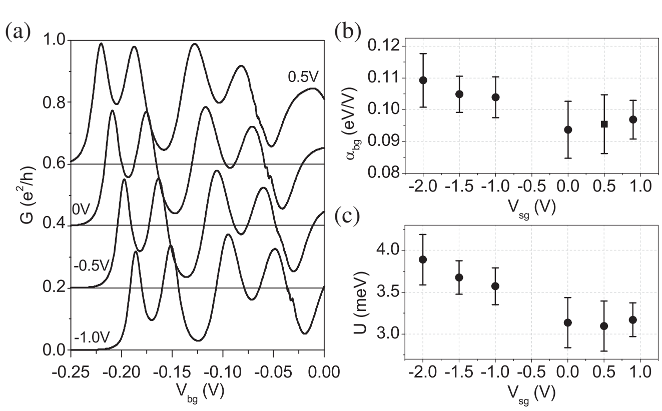


FIG. 2. (a) Plot of $G(V_{bg})$ at $V_{sd} = 0$ V and $B = 0$ T for a range of $V_{sg}$. Curves are offset by $0.2e^2/h$ for clarity. (b) Evaluated $\alpha_{bg}(V_{sg})$. (c) Evaluated $U(V_{sg})$.

electrodes [Fig. 1(a)]. From the stability diagrams, we are unable to observe a significant change in energy level spacing indicating that the changes in confinement when $V_{sg}$ is tuned are small for the states considered.

We now consider the magnetotunneling spectroscopy of the device. The interaction of the electron spins with a magnetic field can be written with the Hamiltonian $\mathcal{H}(t) = \frac{\mu_B}{\hbar}\vec{S} \cdot \hat{g}(V_{sg}) \cdot \vec{B} = \vec{S} \cdot \vec{\Omega}$, where $\hbar$ is Planck's constant, $\vec{S}$ is the electron spin operator, $\vec{\Omega}$ is the spin precession vector, $\hat{g}$ is the $g$ tensor, and $\mu_B$ is the Bohr magneton. We assume that one principal axis of the $g$ tensor is the growth direction of the QD. The in-plane $g$ tensor is then characterized by two in-plane components along two orthogonal in-plane principal axes ($g_{\theta_0}$ and $g_{\theta_0 - 90}$). Here, $\theta_0$ identifies the in-plane principal axes with respect to measurement reference $\theta = 0°$ [see Fig. 1(a)]. The absolute electron Landé $g$ factor is evaluated from the magnetic evolution of the Coulomb peaks, using values of $\alpha_{bg}$ in Fig. 2(b) to convert the splitting of the Coulomb peaks to the Zeeman energy ($E_z = |g|\mu_B B$, where $B$ is the applied magnetic field) [Fig. 1(d)]. For low $B$ fields, the Zeeman splitting is observed to be nonlinear until the Zeeman energy significantly exceeds the orbital separation of the energy levels, following which a linear fit is possible [Fig. 1(d)]. Figures 3(a) and 3(b) show the angular variation of $|g|$ for a range of $V_{sg}$. The measured in-plane absolute $g$ factor as a function of magnetic field angle $\theta$ is described by the elliptical expression[22] $|g| = \sqrt{[g_{\theta_0}\cos(\theta - \theta_0)]^2 + [g_{\theta_0 - 90}\sin(\theta - \theta_0)]^2}$. Example fits to the experimental data are shown in Fig. 3(a). Best fits are achieved for $\theta_0 \sim 0°$, indicating that the principal axes are approximately parallel with the twofold symmetry axes of the elongated QD [see Fig. 1(a)] and correspond with magnetic field angles $\theta \sim 0°$ and $\theta \sim 90°$. These axes also correspond approximately with the [$\bar{1}$10] and [110] cleavage planes of the GaAs substrate as indicated in Fig. 1(a). Note, however, that measurement of a different charge state has shown different anisotropy.[19,20] From SEM images of the device, we observe that the QD is an elongated approximately elliptical structure with width $\sim 100$ nm and length $\sim 200$ nm. For a nonspherical QD, the $g$ tensor components in different directions can differ significantly[23,24] and, subsequently, $g_{\theta_0} \neq g_{\theta_0 - 90}$ in our device. Note that, in a previous study on a small InAs QD device[17] in which single-electron occupation could be achieved, we observed no in-plane anisotropy of $|g|$, indicating the importance of selection of a relatively large and anisotropic QD. We also note that measurements of other charge states reveal different principal-axis directions, indicating that the underlying crystal axes and even geometry may not define the in-plane $g$-factor anisotropy.

The $g$ factor in a QD is strongly influenced by quantum confinement effects,[22,23,25] strain,[26] and composition. We may consider that strong confinement quenches the angular momentum and causes the $g$ factor to approach the free electron value ($g = 2$).[23,24] For weak confinement, the states possess larger angular momentum and the $g$ factor approaches the bulk material value ($g_{\mathrm{InAs}} = -14.7$). For the full picture, we must consider the composition of the QD, specifically the indium concentration profile within the structure as the relative composition of gallium has a significant influence due to the smaller absolute value of the GaAs $g$ factor ($g_{\mathrm{GaAs}} = -0.44$).

Recently, atom probe tomography studies[27–29] on capped self-assembled InAs QDs revealed that the lateral profile of indium concentration was not uniform, but exhibited fluctuation even within a relatively small QD. As no significant change in the energy level spacing is observed, our results appear to indicate that the indium concentration profile of the device is important and that confinement is sufficiently weak that the angular momentum of states is sizable. We therefore conclude that the action of the side-gate electrode is to displace the electron wave function into regions with different material composition (e.g., higher indium content), causing changes in the $g$ factor.

With $\theta$ fixed at 0°, the absolute $g$ factor may be smoothly tuned in the range $|g| = 5.5$–$9$ for the $V_{sg}$ range $-2\,V$–$0.9$ V. This significant variation may be achieved while maintaining the charge state of the QD using the back-gate electrode. Previous papers identified that the effect of $V_{sg}$ on the QD-lead tunnel coupling[18] varies widely for different charge states. Similarly, we find that the variation in $g$ factor varies for different states and even the trend of $g$ factor increasing or decreasing with $V_{sg}$ may be altered when different charge states are measured.[20] For the specific charge state that we focus upon in this paper, we observe that we can alter $|g|$ by $\sim 50\%$ while maintaining the charge state that exceeds previous reports on gated single InAs QDs of $\sim 8\%$.[12] The magnitude of $g$ factor tunability for a single charge state in our device is similar to that recently reported in single InAs nanowire QDs.[30]

For some conditions, we observe that tuning $V_{sg}$ changes not only the magnitude but also the anisotropy of the $g$ tensor. This effect may be observed by measuring the $g$ tensor components for constant $\theta = 0^\circ$ and $\theta = -90^\circ$, which correspond approximately to the in-plane principal axes of the $g$ tensor, giving estimates of the absolute $g$ tensor components $|g_{\theta_0}|$ and $|g_{\theta_0 - 90}|$ [Fig. 3(c)]. Using these data, we evaluate the spin-precession vector $\vec{\Omega}_0$ for the condition $B = 200$ mT and $\theta = 54^\circ$, following Refs. 9,10. The value of $\theta$ is selected to give the largest variation in the spin-precession vector angle ($\phi$) for the $V_{sg}$ range studied. Results are plotted in Fig. 3(d) and reveal a small change in the spin-precession-vector direction for the highest and lowest $V_{sg}$ measured. This indicates that the normalized gradients of the $g$-tensor components with respect to $V_{sg}$ are not equal: $|g_0|'/g_0 \neq |g_{-90}|'/g_{-90}$ where $|g_i|' = \partial|g_i|/\partial V_{sg}$.

The nontrivial dependence of $\hat{g}$ on $V_{sg}$ may be exploited to drive EDSR using the $g$-TMR method described in detail for an ensemble of spins in a two-dimensional system in Ref. 9. Briefly, to achieve $g$-TMR, we may apply a voltage $V_{sg} = V_0 + V_1\cos(\omega t)$ to the side-gate electrode with $\vec{B}$ applied in any direction other than those of the principal axes of the $g$ tensor. The $g$-factor components then vary in time with $g_i(t) = g_i(V_0) + (\partial g_i/\partial V_{sg})V_1\cos(\omega t)$, resulting in a

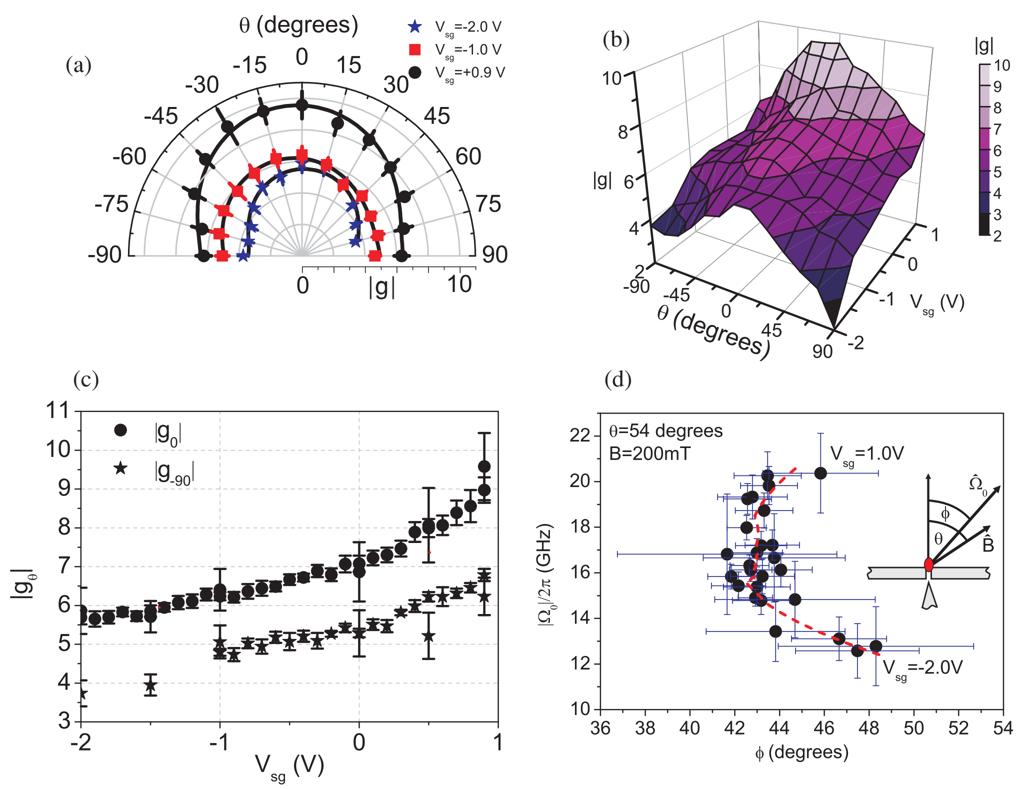


FIG. 3. (Color online) (a) Polar plot of the measured $|g|$ for $V_{sg} = 0.9, -1.0$, and $-2.0$ V. Solid lines indicate best fits using the elliptical expression described in the main text. (b) False color surface plot showing $|g|$ measured as a function of $\theta$ and $V_{sg}$. (c) Plot of $|g_0|(V_{sg})$ and $|g_{-90}|(V_{sg})$, which correspond approximately with the in-plane principal axes of the $g$ tensor. (d) Plot of the evaluated spin-precession vector $\vec{\Omega}_0$ for $B = 200$ mT applied at $\theta = 54^\circ$ evaluated using the data in (c). Each point represents the end point of the precession vector from the origin (0,0). (Inset) Schematic of the in-plane unit vectors $\hat{B}$ and $\hat{\Omega}_0$ with respect to the measurement electrodes. The (red) dashed line represents a spline fit used to predict the potential strength of the g-TMR effect.

time-dependent spin-precession vector $\vec{\Omega} = \vec{\Omega}_0 + \vec{\Omega}_1 \cos(\omega t)$. The time-dependent spin-precession vector ($\vec{\Omega}_1$) may be resolved into components that are parallel [$\vec{\Omega}_\parallel(t)$] and perpendicular [$\vec{\Omega}_\perp(t)$] to $\vec{\Omega}_0$. In the rotating frame, $|\vec{\Omega}_\perp|$ is equivalent to an applied transverse magnetic field, analogous to that which would be used in conventional ESR. The static component of the spin-precession vector [$|\vec{\Omega}_0| = \mu_B |\hat{g}(V_0)| B/h$] determines the Larmor spin-precession frequency and the microwave frequency ($\omega = |\vec{\Omega}_0|$), which needs to be applied to match the static Zeeman splitting and resonantly drive the spin resonance. The Larmor frequency may be tuned by altering $|g|$ with $V_{sg}$ or $\theta$ as well as the magnitude of the external field $B_0$. Note that it is the magnitude of the $g$ factor *anisotropy* that may be induced with the applied side-gate electric field, not the absolute change in $|g|$, which is critical to achieving high Rabi frequencies.

Finally, from the data in Fig. 3(c), we estimate the possible Rabi frequency that we may expect based on the measured $g$ factors and assumptions for some experimentally achievable conditions. We assume a Larmor precession frequency of $|\Omega_0|/2\pi = 20$ GHz, which, for the large $g$ factor of the QD, is achievable for $B$ fields in the range 0.15–0.4 T depending on $V_0$ and $\theta$. For the best conditions for Rabi, we find $V_0 \sim -2$ V and $\theta \sim 54^\circ$ for which $|\Omega_0|/2\pi = 20$ GHz requires $B \sim 0.38$ T. We find that a Rabi frequency of $|\Omega_\perp|/2\pi = 2$ MHz may be achieved for $V_1 \sim 2$ mV. It is likely that these parameters could be significantly improved by changing the design of the device. Selection of a device with smaller $g$ factors (using a smaller QD with higher confinement) would allow the use of higher magnetic fields, which combined with a similar tunability of the $g$ tensor would allow higher Rabi frequencies. Furthermore, the side-gate may be moved closer to the QD and placed such that the source and drain electrodes do not screen the electric field.

In summary, we have shown that a side-gate electrode allows the tuning of the Landé $g$ factor of states in a single InAs quantum dot. We have also discussed how the application of an oscillating electric field may result in an oscillating transverse spin-precession term, allowing resonant control of the spin orientation. The predicted efficiency of the $g$-TMR may be improved through optimized device design by moving side-gate electrode closer to the QD. Further work will be required to investigate the modulation of the $g$ tensor at the gigahertz frequencies required for spin manipulation.

We acknowledge useful discussions with M. Flatté. This work was supported by a Grant-in-Aid for Research S (No. 19104007), A(No. 21244046), and A(No. 22241036), Innovative Areas (No. 21102003), JST strategic Int. Coop. Program, FIRST program, Specially Coordinated Fund from MEXT (NanoQuine), and QuEST Grant No. (HR-001-09-1-0007). Y.K. and S.T. acknowledge financial support from the JSPS young scientist program.

*russell@meso.t.u-tokyo.ac.jp

[1] D. Loss and D. P. DiVincenzo, Phys. Rev. A **57**, 120 (1998).
[2] D. DiVincenzo and D. Loss, J. Magn. Magn. Mater. **200**, 202 (1999).
[3] F. H. L. Koppens, C. Buizert, K. J. Tielrooij, I. T. Vink, K. C. Nowack, T. Meunier, L. P. Kouwenhoven, and L. M. K. Vandersypen, Nature (London) **442**, 766 (2006).
[4] E. I. Rashba and A. L. Efros, Phys. Rev. Lett. **91**, 126405 (2003).
[5] K. Nowack, F. Koppens, Y. Nazarov, and L. Vandersypen, Science **318**, 1430 (2007).
[6] J. Petta, A. Johnson, J. Taylor, E. Laird, A. Yacoby, M. Lukin, C. Marcus, M. Hanson, and A. Gossard, Science **309**, 2180 (2005).
[7] Y. Tokura, W. G. van der Wiel, T. Obata, and S. Tarucha, Phys. Rev. Lett. **96**, 047202 (2006).
[8] M. Pioro-Ladriére, T. Obata, Y. Tokura, Y.-S. Shin, T. Kubo, K. Yoshida, T. Taniyama, and S. Tarucha, Nat. Phys. **4**, 776 (2008).
[9] Y. Kato, R. Myers, D. Driscoll, A. Gossard, J. Levy, and D. Awschalom, Science **299**, 1201 (2003).
[10] J. Pingenot, C. E. Pryor, and M. E. Flatté, Appl. Phys. Lett. **92**, 222502 (2008).
[11] G. Sallis, Y. Kato, K. Ensslin, D. Driscoll, A. Gossard, J. Levy, and D. Awschalom, Nature (London) **414**, 619 (2001).
[12] T. Nakaoka, S. Tarucha, and Y. Arakawa, Phys. Rev. B **76**, 041301(R) (2007).
[13] M. Jung, K. Hirakawa, Y. Kawaguchi, S. Komiyama, S. Ishida, and Y. Arakawa, Appl. Phys. Lett. **86**, 033106 (2005).
[14] M. Jung, T. Machida, K. Hirakawa, S. Komiyama, T. Nakaoka, S. Ishida, and Y. Arakawa, Appl. Phys. Lett. **87**, 203109 (2005).
[15] T. Nakaoka, S. Kako, S. Tarucha, and Y. Arakawa, Appl. Phys. Lett. **90**, 162109 (2007).
[16] G. Katsaros, P. Spathis, M. Stoffel, F. Fourne, M. Mongillo, V. Bouchiat, F. Lefloch, A. Rastelli, O. Schmidt, and S. D. Franceshi, Nat. Nanotechnol. **5**, 458 (2010).
[17] S. Takahashi, R. S. Deacon, K. Yoshida, A. Oiwa, K. Shibata, K. Hirakawa, Y. Tokura, and S. Tarucha, Phys. Rev. Lett. **104**, 246801 (2010).
[18] Y. Kanai, R. S. Deacon, A. Oiwa, K. Yoshida, K. Shibata, K. Hirakawa, and S. Tarucha, Phys. Rev. B **82**, 054512 (2010).
[19] Y. Kanai, R. Deacon, S. Takahashi, A. Oiwa, K. Yoshida, K. Shibata, K. Hirakawa, Y. Tokura, and S. Tarucha, Nature Nanotechnology (in press).
[20] See Supplemental Material at http://link.aps.org/supplemental/10.1103/PhysRevB.84.041302 for additional measurement data.
[21] L. Kouwenhoven, G. Austing, and S. Tarucha, Rep. Prog. Phys. **64**, 701 (2001).
[22] T. P. M. Alegre, F. G. G. Hernández, A. L. C. Pereira, and G. Medeiros-Ribeiro, Phys. Rev. Lett. **97**, 236402 (2006).
[23] C. E. Pryor and M. E. Flatté, Phys. Rev. Lett. **96**, 026804 (2006).
[24] C. E. Pryor and M. E. Flatté, Phys. Rev. Lett. **99**, 179901(E) (2007).
[25] M. T. Björk, A. Fuhrer, A. E. Hansen, M. W. Larsson, L. E. Fröberg, and L. Samuelson, Phys. Rev. B **72**, 201307(R) (2005).
[26] T. Nakaoka, T. Saito, J. Tatebayashi, S. Hirose, T. Usuki, N. Yokoyama, and Y. Arakawa, Phys. Rev. B **71**, 205301 (2005).

[27] M. Müller, A. Cerezo, G. Smith, L. Chang, and S. Gerstl, Appl. Phys. Lett. **92**, 233115 (2008).

[28] M. Müller, D. Saxey, A. Cerezo, and G. Smith, J. Phys.: Conf. Ser. **209**, 012026 (2010).

[29] A. D. Giddings, J. G. Keizer, M. Hara, G. J. Hamhuis, H. Yuasa, H. Fukuzawa, and P. M. Koenraad, Phys. Rev. B **83**, 205308 (2011).

[30] S. Csonka, L. Hofstetter, F. Freitag, S. Oberholzer, and C. Schönenberger, Nano Lett. **8**, 3932 (2008).